



Chemo-immunotherapy by dual-enzyme responsive peptide self-assembling abolish melanoma

Yuhan Wang^{a,b,*}, Limin Xie^b, Xinxin Li^b, Ling Wang^c, Zhimou Yang^b

^a Tianjin Key Laboratory of Inflammation Biology, Department of Pharmacology, School of Basic Medicine, Tianjin Medical University, Tianjin, 300070, PR China

^b Key Laboratory of Bioactive Materials, Ministry of Education, State Key Laboratory of Medicinal Chemical Biology, College of Life Sciences, Collaborative Innovation Center of Chemical Science and Engineering, National Institute of Functional Materials, Nankai University, Tianjin, 300071, PR China

^c State Key Laboratory of Medicinal Chemical Biology, College of Pharmacy, Nankai University, Tianjin 300071, PR China

ARTICLE INFO

Keywords:

Self-assembly
Dual-enzyme responsive
Chemo-immunotherapy
Procedural delivery
Anti-tumor

ABSTRACT

Herein, we designed **Comp. 1** to simultaneously respond to two enzymes: alkaline phosphatase and matrix metalloproteinase 2, which is commonly found in highly malignant cancer cell lines containing B16–F10 murine melanoma cells and CT26 murine colon carcinoma cells. We used the regional differences in the expression levels of dual-markers to accurately release immune molecule IND into tumor microenvironment for the activation of anti-tumor related immune effects, while *in-situ* self-assembly occurs. The dual-enzyme response process can further regulate the peptide precursors' self-assembly in the form of short rod-shaped nanofibers, enabling the delivery of the loaded chemotherapeutic drug HCPT into the cancer cells and further allowing the peptide assemblies to escape from lysosomes and return to cytoplasm in the form of tiny nanoparticles to induce apoptosis of cancer cells. This process does not occur in the single-positive breast cancer cell line MCF-7 or the normal hepatocytes cell line LO2, indicating the selectivity of the cancer cells exhibited using our strategy. *In vivo* studies revealed that **Comp. 1** can effectively cooperate with chemotherapy to enhance the immunotherapy effect and induce immune responses associated with elevated pro-inflammatory cytokines *in vivo* to inhibit malignant tumors growth. Our dual-enzyme responsive chemo-immunotherapy strategy feasible in anti-tumor treatment, provides a new avenue for regulating peptide self-assembly to adapt to diverse tumor properties and may eventually be used for the development of novel multifunctional anti-tumor nanomedicines.

1. Introduction

Cancer plays an important role in the induction of death, anti-tumor treatment has been a topic of concern for researchers [1–5]. However, no symptomatic drugs can be used to implement more targeted treatments for some cancer types with higher malignancy. Although chemotherapy and immunotherapy are widely used in clinical treatment as important means [6–11], some modifications are still needed to compensate for their deficiencies in clinical applications. Due to the poor specificity of traditional chemotherapeutic drugs [12], the most effective way to improve the efficacy of chemotherapy is to effectively deliver enough chemotherapeutic drugs to the diseased site [13–17]. However, it is more likely go off-target to "accidentally injure" the normal tissues and organs *in vivo*, resulting in adverse reactions. Similarly, many

malignant cells are known to develop multiple mechanisms to evade the surveillance of the immune system and induce the formation of an immunosuppressive tumor microenvironment [18–23], while imprecise delivery of drugs for immunotherapy results in greatly reduced efficacy. Furthermore, immunotherapy against tumor growth by awakening dormant immune cells to activate anti-tumor immune responses also needs to be improved owing to the complexity of the immune system, which leads to huge individual differences [24–26]. Although these approaches to anti-tumor treatment have been successful, the development of alternative, efficient strategies to manipulate tumor growth is still emerging [27–31]. The introduction of chemotherapy in immunotherapy has cumulative effect on the control of the disease. On the one hand, chemotherapy effectively inhibits the activity of immunosuppressive cells, such as regulatory T (Treg) cells and myeloid suppressor

Peer review under responsibility of KeAi Communications Co., Ltd.

* Corresponding author. Tianjin Key Laboratory of Inflammation Biology, Department of Pharmacology, School of Basic Medicine, Tianjin Medical University, Tianjin, 300070, PR China.

E-mail address: wangyuhan@tmu.edu.cn (Y. Wang).

<https://doi.org/10.1016/j.bioactmat.2023.09.006>

Received 25 June 2023; Received in revised form 10 September 2023; Accepted 10 September 2023

2452-199X/© 2023 The Authors. Publishing services by Elsevier B.V. on behalf of KeAi Communications Co. Ltd. This is an open access article under the CC BY-NC-ND license (<http://creativecommons.org/licenses/by-nc-nd/4.0/>).

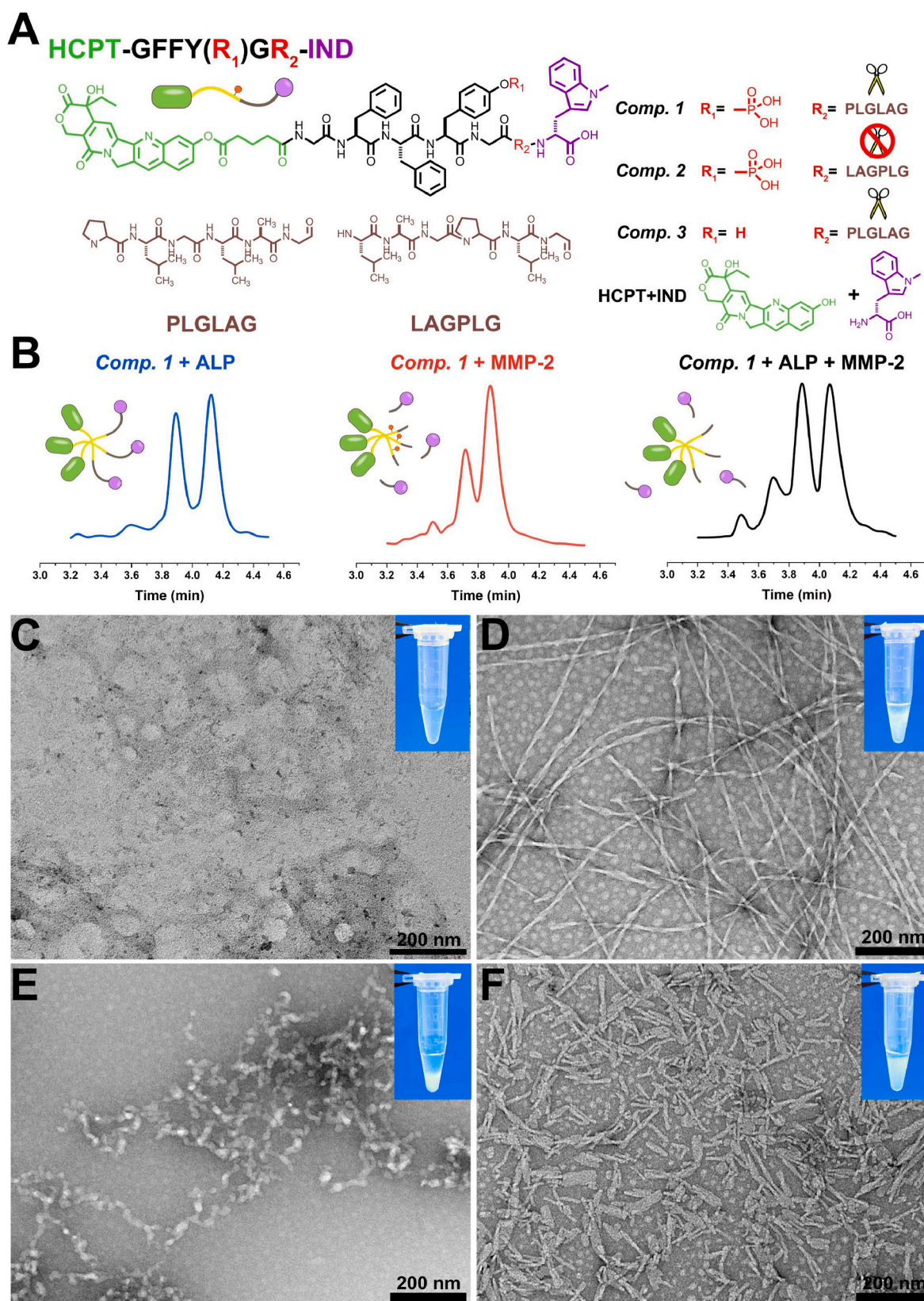


Fig. 1. Molecular design and chemical structure of chemo-immune drug formulations with dual-enzyme responsiveness. (A) Molecular structures of **Comp. 1–3** and the chemotherapeutic drug HCPT, as well as the immune molecule IND. (B) The LC spectrum of **Comp. 1** in the conversion process catalyzed by single or double enzymes and the illustration of the product converted by the above process. TEM and optical images of **Comp. 1** (0.3 wt%) (C) before and after being catalyzed by (D) ALP (5 U/mL), (E) MMP-2 (1 µg/mL), and (F) double enzymes at 37 °C overnight (Black scale bars represent 200 nm).

single or double enzyme catalysis were investigated by transmission electron microscopy (TEM). No noticeable microstructure was observed in **Comp. 1** in the absence of the enzyme. **Comp. 1** formed an intertwined network constructed of slender nanofibers with diameters of 7–10 nm after ALP catalysis, while MMP-2 catalyzed the formation of worm-like nanofibers with diameters ranging from 12 to 15 nm, and short rod-like nanofibers with diameters ranging from 9–15 nm were observed with the simultaneous presence of double enzymes (Fig. 1C–F). Similarly, **Comp. 2** and **3** formed no obvious microstructures before enzymatic catalysis. Among them, **Comp. 2** self-assembled into nanoparticles with diameters of 8–25 nm after catalysis by ALP. Furthermore,

we speculate that **Comp. 3**'s response to MMP-2 is consistent with that of **Comp. 1**'s response to the double enzymes, resulting in a microscopic morphology similar to that of short rod-like nanofibers (Fig. S6). The solution of **Comp. 1** exhibited an emission peak centered at 565 nm with an intensity of 16251 a.u., and the fluorescence intensity showed various degrees of enhancement after catalysis by single or double enzymes, reaching 53027, 25734, and 54533 a.u., which demonstrates the self-assembly behavior of peptide formulations (Fig. S7). Similarly, the fluorescence intensities of **Comp. 2** and **3** also increased after catalysis by ALP or MMP-2 (Fig. S8). We also observed that the critical aggregation concentration (CAC) values for **Comp. 1–3** decreased after

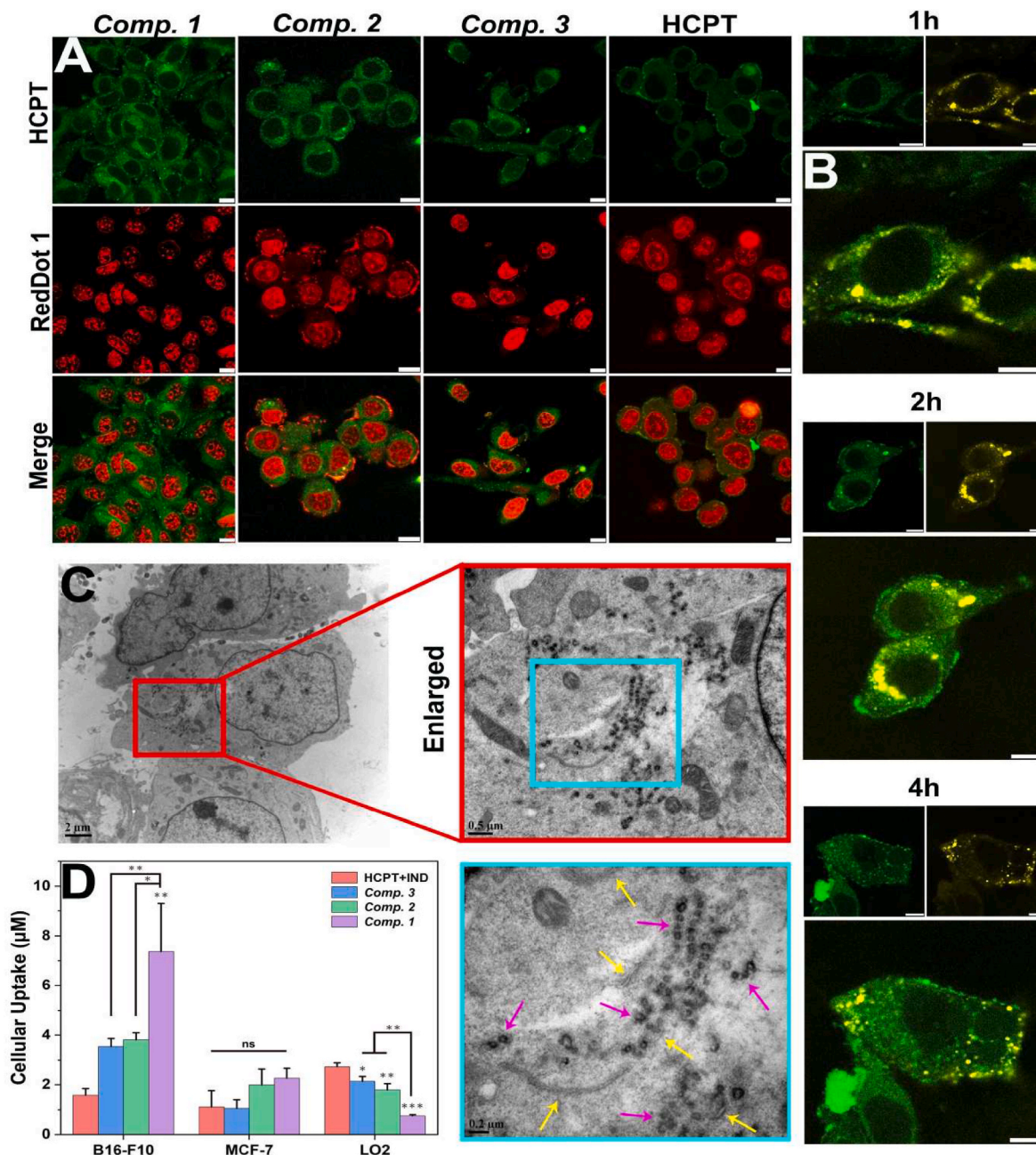


Fig. 2. Cellular uptake and biodistribution of chemo-immunotherapy peptide formulations. (A) CLSM images of B16–F10 cells treated with **Comp. 1–3** and free chemotherapy HCPT for 4 h. (B) Intracellular co-localization of **Comp. 1** and lysosomes in B16–F10 cells after treatment for indicated times ($\lambda_{exc.} = 405$ nm for the green channel of HCPT, $\lambda_{exc.} = 488$ nm for the yellow channel of lysosomes, and $\lambda_{exc.} = 633$ nm for the red channel of RedDot 1). (C) Bio-TEM images of B16–F10 cells incubated with **Comp. 1** for 24 h; yellow arrows mark the nanofibers in the cytoplasm, and pink arrows mark the tiny nanoparticles after the intracellular nanofibers are metabolized by lysosomes. (The scale bars of Bio-TEM are marked in the lower left corner of images.) (D) Cellular uptake of **Comp. 1–3** and free HCPT combined with IND by different cell lines at 4 h time point (The concentration of compounds is 150 μ M, white scale bars represent 10 μ m). The bars shown indicate the mean \pm SE ($n = 3$), and errors were determined using a one-way ANOVA.

enzymatic catalysis, and the CAC value of **Comp. 1** reached 32.95 μM after responding to the double enzymes, indicating that it possesses better self-assembly ability (Figs. S9–S10). At a higher concentration (1 mM), the peptide formulations with slightly negatively charge or nearly neutral charge, thus reducing the adverse loss and nonspecific binding after entering into the systemic circulation (Fig. S11) [57].

2.2. Cell internalization and escape from the lysosomes

Subsequently, we investigated the distribution of **Comp. 1–3** and free HCPT (150 μM) in B16–F10 cells. The results of confocal laser scanning microscopy (CLSM) indicated that a large number of bright green fluorescent spots indicated peptide self-assembly in the cytoplasm of cells treated with **Comp. 1**. However, the relevant fluorescence intensity from HCPT of peptide formulations decreased to varying degrees in cells treated with **Comp. 2** and **3** for the same period of time, and a handful of bright green fluorescent spots were observed in the cytoplasm. The disadvantages of free HCPT, such as its poor solubility, hinder its uptake by cells, and most of the green fluorescence appeared on the cell membrane (Fig. 2A). Effective lysosomal escape and controllable chemotherapy drug unloading are necessary to achieve maximum treatment efficiency, and we examined the lysosomal escape efficiency of **Comp. 1–3** and free HCPT by co-positioning with lysosomes. We found that the fluorescence intensity in the cells incubated with **Comp. 1** was time-dependent. After 1 h of incubation, most of the green fluorescence in cells coincided with the yellow fluorescence, indicating lysosomes. As the incubation time was extended to 2 h, the green fluorescence in the cells was completely covered by yellow fluorescence, indicating that the peptide formulations had entered the lysosomes. When the incubation time reached 4 h, we observed a large number of green fluorescent bright spots that escaped from the lysosomes and returned to the cytoplasm in the form of smaller nanoparticles, whereas **Comp. 2**, **Comp. 3** and free HCPT failed to escape from lysosomes, even after 4 h of incubation with cells (Fig. 2B and Fig. S12). Bio-TEM images of B16–F10 cells showed the presence of nanofibers in the cytoplasm of cells treated with **Comp. 1**, with scattered tiny nanoparticles that were degraded by lysosomes (Fig. 2C and Fig. S13–S14). To explore the effect of the dual-enzyme response on the drug delivery efficiency of peptide formulations, we introduced another two cell lines as control, including MCF-7 breast carcinoma cells, as a single-positive control cell line, and LO2 normal hepatocyte cells, as a double-negative cell line (Fig. S15). Diffuse green fluorescence was observed in the MCF-7 cells incubated with **Comp. 1**, indicating that low expression of a single enzyme affects the assembly morphology of the peptide precursors and the endocytosis efficiency of the cells. For LO2 cells, lower **Comp. 1** entered the cells, and some slightly larger fluorescent bright spots appeared on the cell membrane, which could not be endocytosed by the cells (Fig. S16). Moreover, the co-incubation with **Comp. 1** and two enzyme inhibitors led to a decrease of intracellular fluorescence intensity and a reduction of fluorescent bright spots, which also verified this conjecture (Fig. S17). As shown in Fig. 2D, we investigated the cellular uptake ability of these cell lines for chemo-immunotherapy peptide formulations by measuring the fluorescence intensity of the cell lysates. The cellular uptake of **Comp. 1** by B16–F10 cells was 7.36 μM , which was approximately 3.66-fold higher than free HCPT, indicating the superior drug delivery efficiency of **Comp. 1**.

2.3. In vitro anti-tumor ability

First, we used fluorescence-activated cell sorting (FACS) to determine the ability of different peptide formulations to induce apoptosis. The introduction of **Comp. 2** and **Comp. 3**, as well as free HCPT combined with IND, increased the total apoptosis rate of B16–F10 cells to varying degrees, reaching 49.6%, 38.1% and 26.6%, respectively. Compared with the control group, **Comp. 1** significantly expanded the proportion of early apoptotic cells (13-fold higher than that of PBS

group), apoptotic cells (2.2-fold higher than that of PBS group), further confirming that **Comp. 1** can induce apoptosis of B16–F10 cells to the maximum extent (Fig. 3A–B). Then, we assessed the *in vitro* cytotoxicity of **Comp. 1** on cells. Benefiting from a dual-enzyme response strategy, **Comp. 1** exhibited the strongest cytotoxicity against B16–F10 cells, but not against MCF-7 or LO2 cells, and maintained cell viability at low levels, even at extremely low concentrations (Fig. 3C and Fig. S18). The half-maximal inhibitory concentrations (IC_{50}) of **Comp. 1** on B16–F10 cells were 3.42 μM , which was approximately 2.9-fold lower than **Comp. 2** (13.4 μM), 3.14-fold lower than **Comp. 3** (14.17 μM) and 4.29-fold lower than that of free HCPT (18.09 μM), indicating that **Comp. 1** selectively inhibited the proliferation of B16–F10 cells (Fig. 3D). After confirming the peptide formulations mediated apoptosis in B16–F10 cells, we investigated the expression of pro- or anti-apoptosis proteins to verify the pathway that **Comp. 1–3** induced endogenous cell apoptosis (Fig. 3E–F and Fig. S19). Compared with the control group, the expression levels of apoptosis-related proteins containing p53, p21 and Bax in B16–F10 cells treated with **Comp. 1** increased remarkably, while the expression level of anti-apoptotic protein Bcl-2 decreased. The results suggest that **Comp. 1** may further mediate cell apoptosis by up-regulating p53 pathway.

Next, we investigated the inhibitory effect of **Comp. 1–3** and free HCPT combined with IND on B16–F10 multicellular spheroids (MCSs) constructed *in vitro*. The MCSs in the PBS group maintained continuous growth throughout the period of experiment, reaching 395% of their initial volume after 5 days, indicating a high degree of malignancy. It is shown that the integration of the dual-enzyme responsive peptide precursors with HCPT and IND could remarkably improve the inhibitory effect on simulated solid tumor spheroids *in vitro*. Notably, the MCSs transformed to the unoptimistic growth state promoted by **Comp. 1**, and many apoptotic cell fragments were scattered around spheroids (Fig. 4A). The volumes of the MCSs treated with **Comp. 1–3**, and free HCPT combined with IND exhibited modest reductions of approximately 21, 38, 50 and 52% of the original size, respectively (Fig. 4B). Subsequently, we conducted B16–F10 cell colony formation studies to verify the inhibitory efficiency of peptide formulations on cell proliferation more intuitively. The results showed that whether in free form or in loaded form, the introduction of HCPT significantly inhibited the cell colony formation. While the cells treated with **Comp. 1** were more difficult to form colonies, indicating that **Comp. 1** with dual-enzyme responsiveness is more destructive to cell proliferation and survival. (Fig. 4C).

2.4. In vivo anti-tumor efficacy and biological safety assessment

We evaluated the inhibitory effect of the peptide formulations on the IDO-1 enzyme by analyzing extracellular Kyn inhibition, which is an important indicator of IDO enzyme bioactivity. As shown in Fig. 5A, the treatment with **Comp. 1–3** and free IND at a concentration of 150 μM was the most effective in inhibiting the production of Kyn in a concentration-dependent manner. Inhibition rates of Kyn treated with **Comp. 1–3** and free IND reached 38.04, 28.66, 31.34, and 25.93%, respectively. It is worth noting that the effects of **Comp. 1** and **3** are better than those of **Comp. 2**, which demonstrated that the cleavage response induced by MMP-2 was more conducive to the release of the immune molecule IND in the microenvironment. In order to observe the distribution of the peptide formulations after entered the tumor-bearing mice more intuitively, we used Cy5.5, a near infrared fluorescent dye, to fluorescently label the peptide formulations for *in vivo* fluorescence imaging. By constructing xenograft CT26 tumor-bearing mice, we injected Cy5.5-labeled **Comp. 1–3** and free Cy5.5 intravenously for imaging using *In Vivo* Imaging System (IVIS) (Fig. 5B). **Comp. 1** exhibited that the concentrate signal accumulation in the tumor site of mice within 2 h, and further realizing long-term retention until 72 h. However, although the fluorescence signal of **Comp. 2** also gathered in the tumor site with the systemic circulation *in vivo*, which were

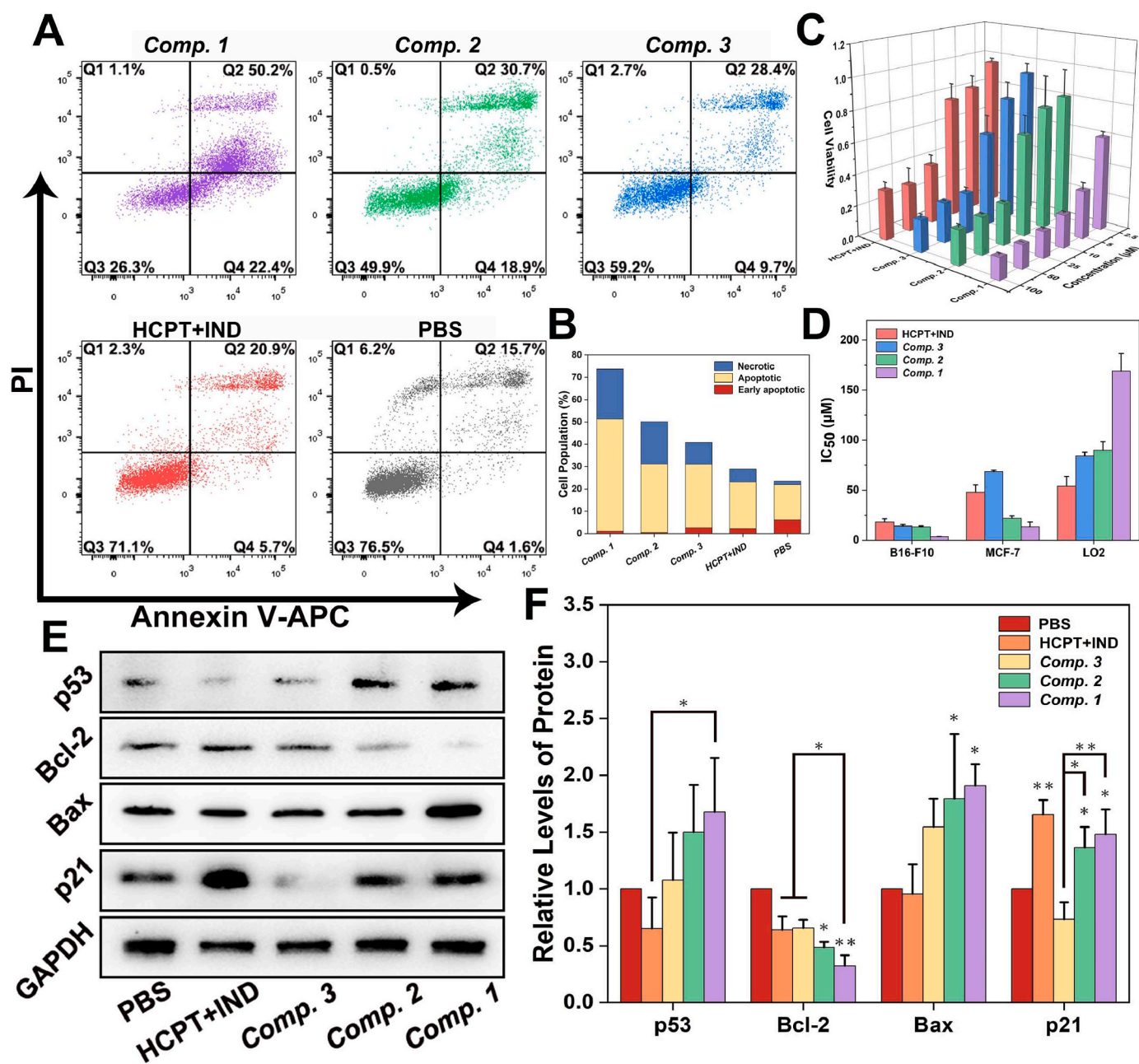


Fig. 3. *In vitro* therapeutic effect of chemo-immunotherapy peptide formulations. (A) APC-Annexin V/PI staining assays of B16-F10 cells after incubation with 150 μM of different formulations for 24 h. (B) Population of early apoptosis, apoptosis, and necrosis in B16-F10 cells treated with different formulations. (C) Cell viability of B16-F10 cells incubated with **Comp. 1–3** and free HCPT combined with IND at indicated concentrations for 48 h. (D) IC₅₀ values of different cell lines incubated with **Comp. 1–3** and free HCPT combined with IND (150 μM) for 48 h. (E) Western blots of cell apoptosis related factors in B16-F10 cells incubated with indicated formulations for 24 h. (F) Quantitative analysis of p53, Bcl-2, Bax and p21 expression levels in (E). Adjusting according to GAPDH. The bars shown are the mean \pm SE ($n = 3$), and errors were determined using a one-way ANOVA.

metabolized rapidly due to its limited permeability. Instead, **Comp. 3** and free Cy5.5 did not show their enrichment in tumor sites. Then, *in vitro* imaging of the isolated B16-F10 tumor tissues and homogenate also verified that **Comp. 1** owns superior tumor site targeting and enrichment efficiency *in vivo*, and the fluorescence signal intensity of tumor sites in mice treated with **Comp. 1** was particularly higher than that in other groups, which proved its universality in specific targeting of double-positive tumors (Fig. 5C and Fig. S20). More than that, the red fluorescence indicated by peptide formulations in tumor tissues isolated from mice administered with **Comp. 1** almost filled the cytoplasm of tumor cells in the field of vision, **Comp. 2** and **Comp. 3** were relatively less, while free Cy5.5 was difficult to enter into the tumor cells due to its

lack of targeting sequence and assembly ability (Fig. S21). We then evaluated the *in vivo* anti-tumor properties of the peptide formulations (Fig. 5E). In comparison to the groups of PBS and free HCPT combined with IND, four doses of tail vein administration of **Comp. 1** could significantly inhibit the tumor growth rate and still showed an extraordinary inhibitory effect in the late stage with exponential growth of tumors (Fig. S22). The average volume of the tumors treated with **Comp. 1** increased slightly to $\sim 504 \text{ mm}^3$ at the end of monitoring, which was equivalent to only 0.21-fold by that of the PBS group. However, the growth rate of tumors in mice treated with **Comp. 2–3** and free HCPT combined with IND continued to increase during the experimental period, and finally the average volumes reached $\sim 1018 \text{ mm}^3$

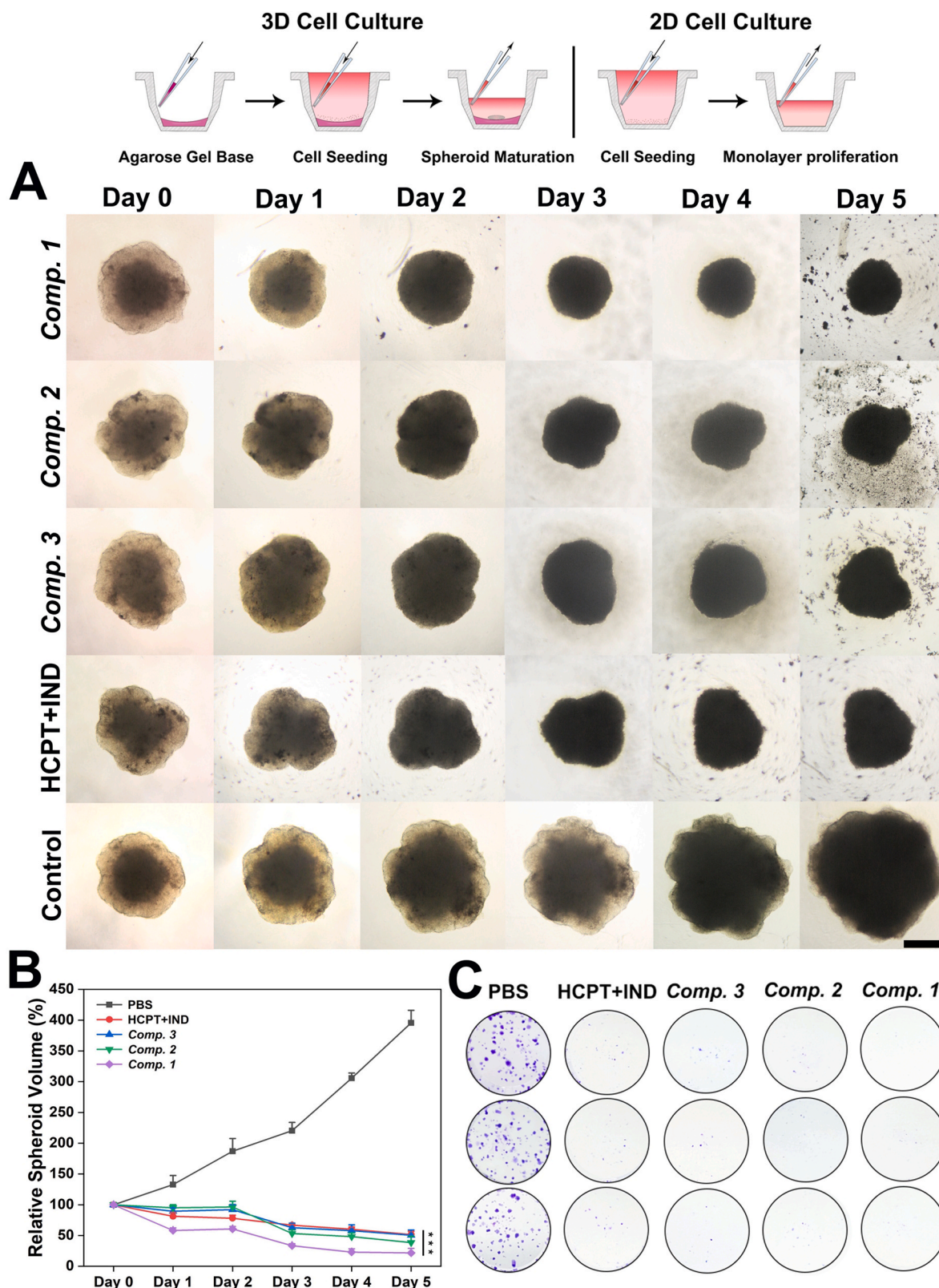
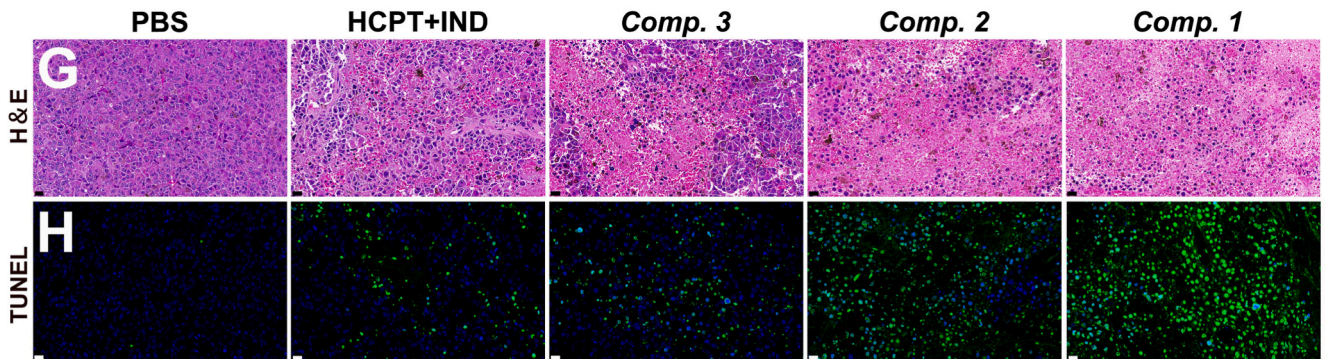
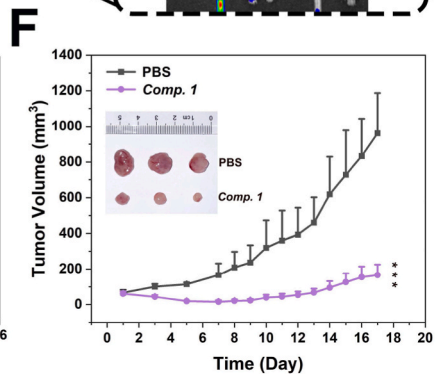
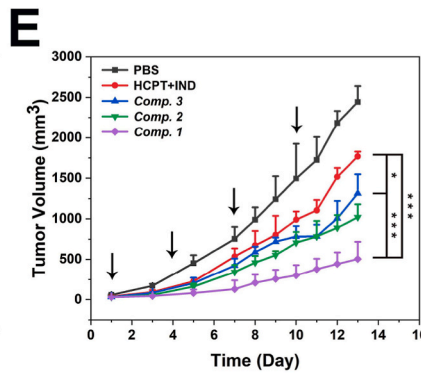
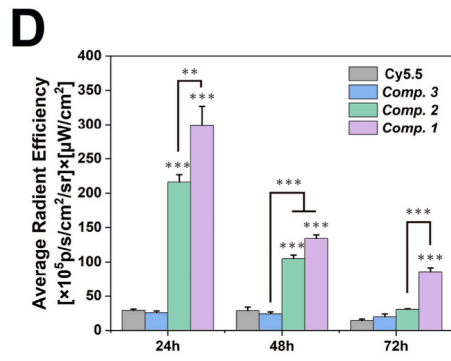
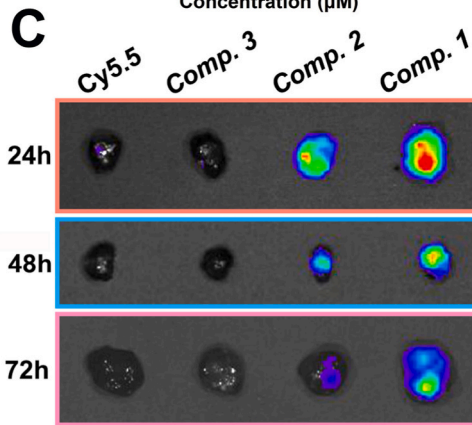
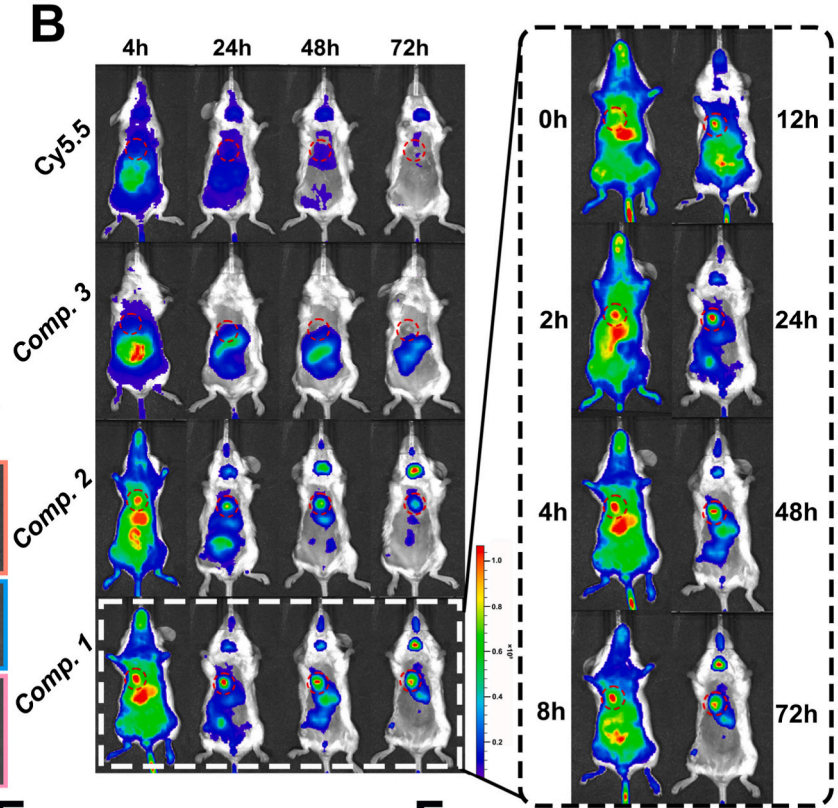
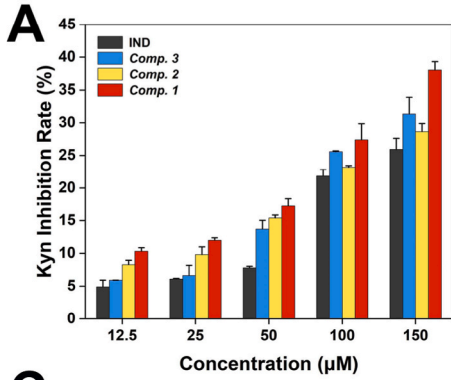
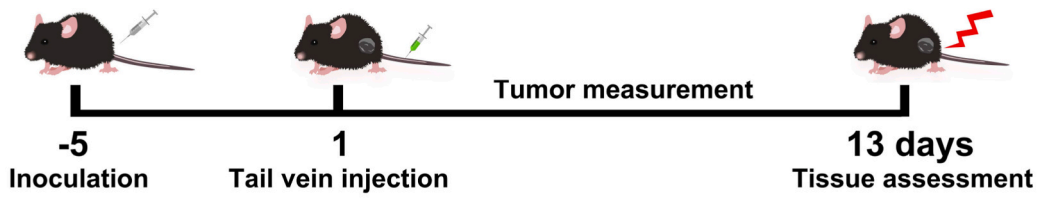


Fig. 4. Effect of chemo-immunotherapy peptide formulations on the growth and formation of simulated tumor spheroids. (A) Optical images of B16–F10 3D MCSs' growth after treatment with different compounds (150 μ M), the spheroids treated with drug-free medium served as controls (Black scale bars represent 100 μ m). (B) The volume of B16–F10 MCSs in each group at different time points were compared with their initial volume. (C) Colony formation photographs of B16–F10 cells treated with the indicated formulations (150 μ M) for 24 h. The bars shown are the mean \pm SE (n = 3), and errors were determined using a one-way ANOVA.



(caption on next page)

Fig. 5. *In vivo* anti-tumor efficacy of chemo-immunotherapy peptide formulations. (A) Kyn inhibition rate of each peptide preparation against IDO immune pathway in B16–F10 cells. (B) *In vivo* near-infrared fluorescence imaging of BALB/c mice bearing CT26 xenografts after intravenous administration of different formulations at the indicated time points. (The red dotted circles indicate the subcutaneous tumor sites and the black rectangle on the right shows the extended fluorescence images for **Comp. 1**.) (C) *Ex vivo* fluorescence imaging of isolated B16–F10 tumors from mice injected with Cy5.5-labeled **Comp. 1–3** and free Cy5.5 after 24 h (orange border), 48 h (blue border), 72 h (pink border). (D) The fluorescence statistical results of (C). The monitoring results of the growth of (E) B16–F10 tumors in C57BL/6 mice and (F) CT26 tumors in BALB/c mice in response to the treatment of **Comp. 1–3** and free HCPT combined with IND, the injection dose is equivalent to 3 mg/kg HCPT. The results of (G) H&E staining and (H) TUNEL staining of tumor tissue sections from mice in different groups. ($\lambda_{exc.} = 488$ nm for green channel, and $\lambda_{exc.} = 405$ nm for blue channel of DAPI. Both black and white scale bars represent 20 μ m) The bars shown are the mean \pm SE (n = 5), and errors were determined using a one-way ANOVA.

(**Comp. 2**), ~ 1314 mm³ (**Comp. 3**), and approximately 1767 mm³ (HCPT + IND), respectively (Figs. S23–S25). Moreover, the monitoring of the average body weight of the mice in each group during the experimental period revealed no abnormalities, confirming the biosafety of our treatment (Fig. S26). CT26, as another double-positive cell line, used to re-verify the anti-tumor performance of **Comp. 1** *in vivo*. As shown in Fig. 5F, in the subcutaneous tumor model with the same initial volume as the control group, the tumor growth of mice stimulated by **Comp. 1** was well suppressed, and finally the average volume was

controlled to about 0.17-fold by that of the PBS group.

We then used hematoxylin-eosin (H&E) staining to investigate the physiological state of tumor tissues isolated from mice in each group to further evaluate the anti-tumor efficacy of different peptide formulations. As shown in Fig. 5G, the nuclei distributed in the tumor tissues of the PBS group were dense and uniform. In contrast, the distribution of cells in the tumor tissues of **Comp. 1** group was sparser, and the nuclei were severely fragmented. In addition, the results of TdT-mediated dUTP nick end labeling (TUNEL) staining, which can indicate

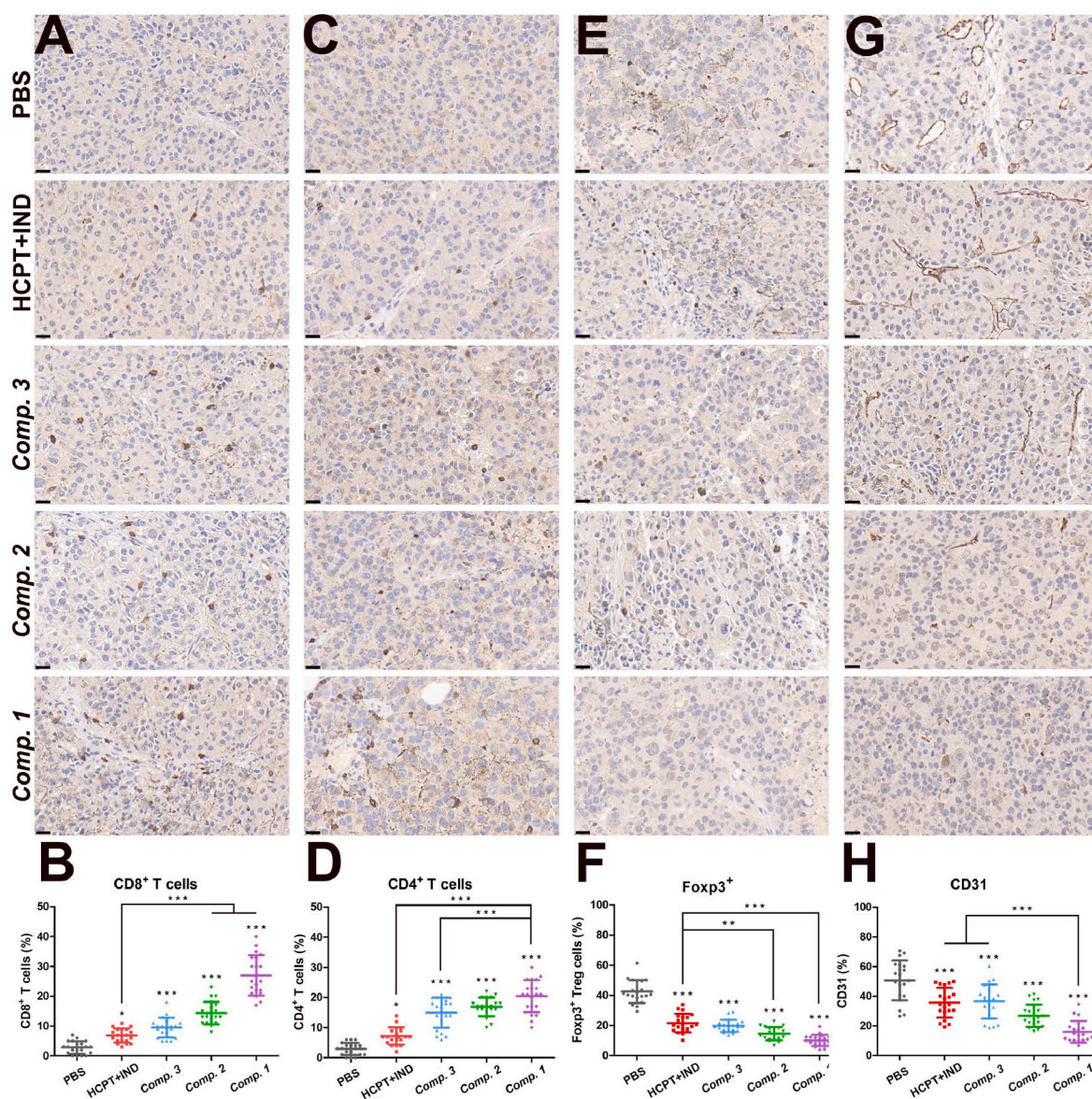


Fig. 6. The infiltration of immune cells in tumor tissues using IHC. IHC staining results and statistical analysis of (A)–(B) cytotoxic CD8⁺ T cells; (C)–(D) helper CD4⁺ T cells; (E)–(F) Foxp3⁺ Treg cells infiltrated in tumor tissues and (G)–(H) CD31⁺ cells indicating tumor vascular endothelial differentiation (Scale bars represent 20 μ m). The bars shown are the mean \pm SE (n = 20), and errors were determined using a one-way ANOVA.

apoptotic cells in the tumor tissue, showed that there were a large number of apoptotic cells in the tumor tissues of **Comp. 1** group, whereas almost no apoptotic cells were observed in the PBS group (Fig. 5H). Although the aggregation of peptide formulations in major organs could be observed, we further assessed the systemic toxicity of all formulations using histological and hematological analysis. The results of H&E staining of major organs showed that compared with the PBS group, no obvious cell damage or morphological changes were observed in each group treated with peptide formulations (Fig. S27). Next, we collected blood from mice in each group for hematological assessments, demonstrating the negligible systemic toxicity of the drug–peptide conjugates, and the adverse events caused by free HCPT were rescued (Fig. S28–S29). These observations suggest that although no significant damage was observed by histology, the systemic toxicity of free HCPT was still present and the peptide formulation could neutralize its toxic side effects.

2.5. Immune effect of peptide formulations *in vivo*

To reveal the immune effect of our designed peptide formulations in the anti-tumor process *in vivo*, we detected cytotoxic CD8⁺ T cells, helper CD4⁺ T cells, regulatory Foxp3⁺ Treg cells, and CD31 positive indicators in tumor tissues treated with different peptide formulations by immunohistochemical (IHC) staining to reveal the infiltration of specific tumor-related lymphocytes and angiogenesis in tumor tissues. As shown in Fig. 6, among all tested peptide formulations, **Comp. 1** was able to effectively induce an increase in the number of CD8⁺ T cells and CD4⁺ T cells infiltrating the tumor tissues. However, the staining results for Foxp3⁺ Treg cells, which can trigger immunosuppression, were the opposite. The increase in anti-tumor immune-specific T cells and fewer regulatory T cells are more conducive to tumor killing and remission of related immunosuppression. Thus, we believe that **Comp. 1** can induce anti-tumor immune effects that cooperate with the immune system to inhibit tumor growth. In addition, we detected CD31 positive indicators in tumor tissues from each group and found that large positive areas appeared in the tumor tissues of the PBS group, indicating that the blood vessels were densely distributed and the blood flow was abundant, indicating that the tumors were adequately supplied with nutrients and grew rapidly at this time. However, almost no positive region was observed in **Comp. 1** group's tumor tissues, indicating that **Comp. 1** had a remarkable inhibitory effect on the malignant proliferation of the B16–F10 tumors. The corresponding quantitative analysis results were consistent with the observations.

Next, we explored the mechanism by which the peptide formulations exerted anti-tumor immunity. We first determined the immune response induced by peptide formulations by measuring the DC maturation *in vitro* (Fig. 7A–B). After bone marrow dendritic cells (BMDCs) were co-cultured with B16–F10 cells pretreated with **Comp. 1–3** and free HCPT combined with IND, **Comp. 1** significantly triggered the maturation of BMDCs, which was 2.3-fold higher by that of the control group. Moreover, the proportion of DC maturation induced by **Comp. 1** was almost the same as that of the lipopolysaccharide (LPS) pretreatment group, which verifies **Comp. 1**-induced immune response *in vitro*. After we obtained a new batch of tumor-bearing mice according to the tumor model construction method in the *in vivo* anti-tumor experiment, following the same dosage with three administrations by tail vein injection. We collected tumor tissues from mice of each group at 24 h after the last administration, and the growth trend of tumors was basically the same as the previous results (Fig. S30). Simultaneously, we extracted fresh splenocytes from mice in each group and detected the proportion of specific tumor-related lymphocytes after stimulating by **Comp. 1–3** and free HCPT combined with IND using FACS (Fig. 7C and Figs. S31–S32). The optimal induction was observed in the mice in response to **Comp. 1**, the ratios of cytotoxic CD8⁺ T cells to helper CD4⁺ T cells reached 2.63- and 1.96-fold, respectively in splenocytes of **Comp. 1**-treated mice compared to that in the PBS group. Furthermore, less

proportion of MDSCs (Gr-1⁺ CD11b⁺ cells) and Treg cells (CD25⁺ Foxp3⁺ cells in CD3⁺ CD4⁺ population) capable of mediating immunosuppression were observed in mice stimulated by **Comp. 1**, which respectively were 37.98 and 17.96% lower than those in PBS group, indicating that **Comp. 1** can effectively inhibit the recruitment of MDSCs and the activation of Treg cells. Similarly, we also observed significant increase in the infiltration of CD8⁺ and CD4⁺ T cells from the results of FACS in lymphocytes isolated from tumor tissues of mice treated with **Comp. 1**, whereas the proportion of MDSCs and Treg cells decreased remarkably (Fig. S33). We believe that the immune response induced by chemo-immunotherapy peptide formulations is critical, and that the dual-enzyme response process plays an indispensable role in the anti-tumor process.

Moreover, we measured several key pro-inflammatory cytokines (IFN- γ , IL-2, IL-6, IL-12, and TNF- α) in the serum obtained from the tumor-bearing mice using enzyme-linked immunosorbent assay (ELISA) to investigate whether chemo-immunotherapy peptide formulations could induce the elevated levels of cytokines to activate the relevant anti-tumor immune response. As shown in Fig. 7D, the average expression levels of cytokines in **Comp. 1**'s group respectively increased by 1.57-, 14.62-, 10.25-, 8.23-, and 4.66-fold, compared to the control group. However, the other peptide formulations and free HCPT combined with IND exhibited a slight induction effect that boosted the increase in these cytokines. Protective memory T cells play an important role in the prevention and treatment of many diseases, which are divided into native memory T (T_n) cells, central memory T (T_{CM}) cells and effector memory T (T_{EM}) cells at least. We used coordinate analysis of CD44 and CD62L expression by CD8⁺ and CD4⁺ T cells in splenocytes to precisely define how T_n, T_{CM}, and T_{EM} cell subsets are organized within an individual (Fig. 7E). Analysis of CD8⁺ and CD4⁺ T cell subsets both revealed that mice stimulated by **Comp. 1** can produce a higher proportion of T_{EM}, which provides a long-term or even lifelong sustained immune response for the body, while the control group is dominated by unactivated T_n cells. These results confirmed that **Comp. 1** could effectively induce an increase in pro-inflammatory cytokines *in vivo*, further activate tumor-adaptive immune responses, and cooperate with chemotherapeutic drug HCPT to participate in the anti-tumor process.

3. Conclusions

We proposed a novel strategy utilizing a dual-enzyme response to construct chemoimmunotherapeutic peptide formulations. Most tumor cells, including B16–F10 cells, exhibit extracellular ALP expression, and MMP-2 is commonly found in the extracellular microenvironment of some highly malignant tumor cells. In this study, we used several chemo-immunotherapy peptide formulations (**Comp. 1–3**) to investigate their effects on anti-tumor activity and the activation of tumor-associated immune responses. Extracellular ALP and MMP-2 effectively regulate the *in situ* self-assembly of **Comp. 1** to form nanofibers that are endocytosed into tumor cells while releasing the immune molecule IND into the tumor microenvironment to induce anti-tumor immune effects. The realization of lysosomal escape plays an important role in improving the bioavailability of drugs. **Comp. 1** escapes after entering lysosomes and returns to the cytoplasm in the form of tiny nanoparticles to induce apoptosis in cancer cells. We used a dual-enzyme response strategy to regulate the self-assembly of peptide formulations, organically combined chemotherapy with immunotherapy, which showed excellent efficacy in tumor treatment. We hypothesized that our proposed dual-enzyme responsive chemo-immunotherapy approach has substantial potential for the development of multifunctional anti-tumor nanomedicines.

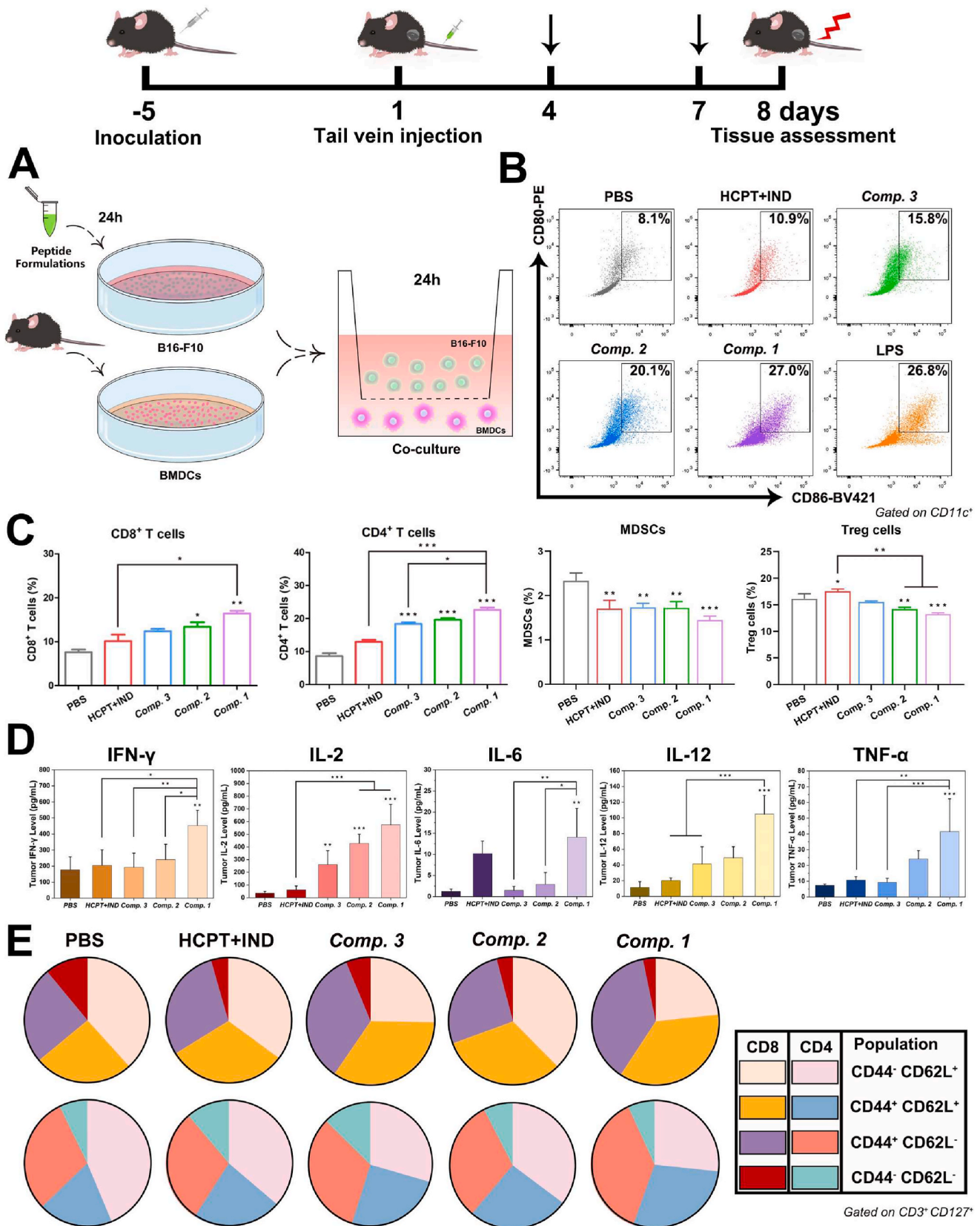


Fig. 7. The effect of chemo-immunotherapy peptide formulations on cytokine-related immune responses in mice. (A) Schematic illustration of the DC maturation assay *in vitro*. (B) *Comp. 1–3* and free HCPT combined with IND induced DC maturation *in vitro*. The LPS-pretreated group was used as the positive control. (C) Flow cytometric quantification of CD8⁺ T lymphocytes, CD4⁺ helper T lymphocytes, MDSCs and Treg cells among splenocytes after *in vivo* stimulation via tail vein administrations. (D) Cytokine levels of IFN- γ , IL-2, IL-6, IL-12 and TNF- α in serum of mice from different groups detected by ELISA after *in vivo* stimulation via tail vein administrations. (E) The average frequency of memory CD8⁺ (top) and CD4⁺ (bottom) T cells (T_N: CD44⁻ CD62L⁺, T_{CM}: CD44⁺ CD62L⁺, T_{EM}: CD44⁺ CD62L⁻). The dosage is consistent with the anti-tumor experiment. The bars shown are the mean \pm SE (n = 3), and errors were determined using a one-way ANOVA.

4. Methods

4.1. Preparation of peptide derivatives

All peptide derivatives were prepared using the conventional Fmoc-based SPPS with 2-chlorotrityl chloride resin. The corresponding N-Fmoc-protected amino acids were added to the system. Benzotriazole-N, N',N'-tetramethyluronium hexafluorophosphate (HBTU) was used as the coupling reagent to couple with the free amino group of the next Fmoc-protected amino acid. In the final coupling step, glutaric anhydride 10-hydroxycamptothecin (HCPT-GA) was used to produce the chemo-immune drug formulations. The peptide derivatives were cleaved using 95% trifluoroacetic acid (TFA) containing 2.5% triisopropylsilane (TIS) and 2.5% H₂O. Next, ice-cold anhydrous was added to the lysis reagent, the solvent was evaporated, and the resulting precipitate was the crude peptide derivative. The obtained solid powder was dissolved in dimethyl sulfoxide (DMSO) and separated by HPLC to obtain the corresponding pure product.

4.2. Construction of self-assembly system

We weighed 3 mg of each compound and fully dissolved it in 1 ml of 1 × PBS to obtain a 0.3 wt% solution of peptide precursor molecules for subsequent experiments. If the concentration of formulations required for the experiment is different from it, dilute it from this concentration. The dosage of ALP added was 5 U/mL, and MMP-2 needed to be activated by 4-aminophenyl mercuric acetate (APMA, working concentration of 10 mM) in advance, and then added to an equal volume as the peptide precursor solution (final concentration was 1 µg/mL).

4.3. Fluorescence detection of intracellular distribution

B16–F10 cells were inoculated in a small Petri dish at an appropriate cell density. After the cells were attached to the bottom of a small Petri dish, the solution of free HCPT combined with IND, and **Comp. 1–3** (150 µM) was added to incubate the cells for different periods of time. Next, lysosomal dye and RedDot 1 were used to stain cells with lysosomes and nuclei. After removing the stain, the samples were observed with CLSM (Leica TSC SP8). All these operations are protected from light.

4.4. Confirmation of intracellular distribution by bio-TEM

We inoculated B16–F10 cells in a cell culture dish at an appropriate density. After 24 h, the cells adhered to the bottom of the dish evenly. Next, cells were incubated with **Comp. 1** (150 µM) for another 24 h. At the end of incubation time, the culture medium containing peptide derivatives was removed and gently washed with PBS buffer for three times. We use a cell scraper to collect the cells attached to the bottom of the dish, and discard the supernatant after centrifugation. Cell precipitation was dehydrated after fixation, which then embedded in ultrathin sections, and stained with lead citrate solution and uranyl acetate in 50% ethanol saturated solution, finally observed by TEM.

4.5. Cell apoptosis analysis

To evaluate the ability of different peptide formulations (**Comp. 1–3** and free HCPT combined with IND), to induce apoptosis, FACS was carried out to obtain the results of annexin V and PI double staining. We seeded B16–F10 cells in a 6-well plate at a density of 2×10^5 cells per well. Then, we added peptide formulations respectively to each well and continued to incubate for 24 h. After the incubation, the cells were harvested, resuspended by binding buffer and stained with Annexin-APC/PI for 30 min. The numbers of early apoptosis (Annexin V-APC positive), apoptosis (Annexin V and PI double positive) and necrosis (PI positive) cells were analyzed by flow cytometer (BD LSRFortessa).

4.6. Western blotting

The total protein in cell samples was lysed with Radio immunoprecipitation buffer (RIPA) containing protease inhibitor. Protein concentration was determined by Bicinchoninic acid (BCA) quantitative determination method, and the loading amount was 20 µg. Lysates containing equal amount of protein were separated by 15% or 10% SDS-PAGE and transferred to polyvinylidene fluoride membrane (Millipore). 5% of skim milk was used for blocking and then incubated with primary antibody at 4 °C overnight. Primary antibodies against the following protein were used: p53 (60283-2-Ig, Proteintech); Bcl-2 (68103-1-Ig, Proteintech); Bax (50599-2-Ig, Proteintech); p21 (28248-1-AP, Proteintech). The membrane was incubated with HRP-labeled secondary antibody at room temperature for 2 h. Blots were exposed and imaged by Tanon imaging system (5200Multi).

4.7. MCSs studies

The solution was prepared by adding 0.2 g of agarose to each 10 mL of dulbecco's modified eagle medium (DMEM), autoclaving at 120 °C for 20 min, and then immediately adding 50 µL of agarose solution to each well of the 96-well plate. After the agarose cooled and solidified, B16–F10 cells containing complete medium were added to the wells. The agarose gel at the bottom of the plate prevented the cells from adhering to the wells [58]. After the B16–F10 3D MCSs were constructed, **Comp. 1–3** and free HCPT combined with IND at a concentration of 150 µM to incubate MCSs, and the drug-containing medium was replaced every two days, the untreated group was used as a control. We recorded the sizes of the MCSs in different groups at the indicated time points after adding the chemo-immune drug formulations.

4.8. Cell colony formation studies

B16–F10 cells in logarithmic growth phase were digested and resuspended into cell suspension, then counted and inoculated into 12-well plates at the density of 1×10^3 cells per well. After the cells in the well adhered to the wall and grew steadily (about 3 days), we continued to culture the cells for 24 h with complete medium containing peptide formulations (**Comp. 1–3** and free HCPT combined with IND). After the treatment, it was replaced with fresh medium and continued to culture until the number of cells in most single clones is more than 50. Then, 4% paraformaldehyde was added and fixed cells for 30–60 min, then crystal violet dye solution was added to each well to stain the cells for 10–20 min. The cells were washed several times with PBS buffer, dried and photographed with a digital camera.

4.9. Kyn inhibition

The inhibitory effects of **Comp. 1–3** and free IND on the IDO-1 enzyme *in vitro*. First, we inoculated B16–F10 cells into the well plate with appropriate density. After the cells adhered to the bottom of plate, solution of **Comp. 1–3** and free IND containing IFN-γ (50 ng/mL) were added to each test well. After the incubation time of 48 h, we carefully transferred the supernatant to a new well plate. Next, trichloroacetic acid (30%) was added to each reaction well and incubated at 50 °C for 30 min. This process converts N-formyl kynurenine into kynurenine. Then, we centrifuged the well plate and transferred the supernatant to a new well plate, and added an appropriate amount of Ehrlich reagent to each test well, and incubate at 25 °C for 10 min. Finally, we measured the optical density (OD) at 490 nm with a multifunctional iMark microplate reader (Bio-Rad, USA).

4.10. In vivo anti-tumor experiments

We selected C57BL/6 mice (6–8 weeks old, about 20 g) and BALB/c mice (8 weeks old, about 20 g) as experimental animals in this study.

B16–F10 cells (7×10^5 cells per mouse) and CT26 cells (1×10^6 cells per mouse) were inoculated subcutaneously in the chest of mice, respectively. When the average tumor volume of mice reached about 60–70 mm³, all tumor-bearing mice in each group ($n = 5$) were treated with different peptide precursors by tail vein injection. Taking the free HCPT dose of 3 mg/kg per mouse as a reference, the injection dose of each preparation was calculated according to the molecular weight. The tail vein of each mouse was injected every three days, three times in total, and the indexes of mice in each group were monitored. Use the following formula to calculate the tumor volume: (volume = width² × length × 0.5). At the end of the experiment, the mice were sacrificed by neck removal. The tumors and organ tissues were dissected for further H&E staining, TUNEL cell apoptosis staining and analysis by IHC.

4.11. DC maturation *in vitro*

To detect DC maturation induced *in vitro*, we isolated BMDCs from C57BL/6 mice. First, 1×10^5 of B16F10 cells were co-incubated with **Comp. 1–3**, HCPT combined with IND, and LPS (as a positive control) to obtain pretreatment. Subsequently, the B16F10 cells were harvested and incubated with the isolated BMDCs for 24 h, then BMDCs were collected and stained with anti-CD11c-FITC, anti-CD80-PE and anti-CD86-BV421, and the mature dendritic cells were analyzed by flow cytometer (BD LSRFortessa).

4.12. Determination of cytokine production in the blood of mice

According to the method described above, C57BL/6 mice (6–8 weeks old, about 20 g) were inoculated subcutaneously with B16–F10 tumor in the chest of mice, which were injected with various peptide precursors through tail vein, and the injection dose was consistent with the antitumor experiment. 24 h after the last administration, we collected serum samples from each group of mice, the OD values were carried out, and the levels of cytokines in serum were obtained by substituting them into the standard curve equation.

Ethics approval and consent to participate

All the animal care and experimental protocols were performed in agreement with the rules of the Animal Ethical and Experimental Committee of the Tianjin Medical University (Tianjin, China) and the Animal Ethical and Experimental Committee of the Nankai University (Tianjin, China). This work does not use human subjects.

CRedit authorship contribution statement

Yuhan Wang: Methodology, Validation, Formal analysis, Investigation, Data curation, Visualization, Writing – original draft, Project administration, Funding acquisition. **Limin Xie:** Methodology, Validation, Formal analysis, Investigation, Data curation. **Xinxin Li:** Methodology, Investigation. **Ling Wang:** Conceptualization, Writing – review & editing, Supervision, Project administration, Funding acquisition. **Zhimou Yang:** Conceptualization, Writing – review & editing, Supervision, Project administration, Funding acquisition.

Declaration of competing interest

The authors declare no conflict of interest.

Acknowledgements

This work was supported by the National Key Research and Development Program of China (2022YFB3804600), the National Natural Science Foundation of China (32171325, 32301122 and 82261160656).

Appendix A. Supplementary data

Supplementary data to this article can be found online at <https://doi.org/10.1016/j.bioactmat.2023.09.006>.

References

- [1] X.G. Zhang, J.J. Tang, C. Li, Y. Lu, L.L. Cheng, J. Liu, A targeting black phosphorus nanoparticle based immune cells nano-regulator for photodynamic/photothermal and photo-immunotherapy, *Bioact. Mater.* 6 (2021) 472–489.
- [2] J.J. Shi, P.W. Kantoff, R. Wooster, O.C. Farokhzad, Cancer nanomedicine: progress, challenges and opportunities, *Nat. Rev. Cancer* 17 (2017) 20–37.
- [3] S.K. Li, W.J. Zhang, R.R. Xing, C.Q. Yuan, H.D. Xue, X.H. Yan, Supramolecular nanofibrils formed by coassembly of clinically approved drugs for tumor photothermal immunotherapy, *Adv. Mater.* 33 (2021), 2100595.
- [4] B.B. Sun, R. Chang, S.P. Cao, C.Q. Yuan, L.Y. Zhao, H.W. Yang, J.B. Li, X.H. Yan, J. C.M. van Hest, Acid-activatable transmorphic peptide-based nanomaterials for photodynamic therapy, *Angew. Chem. Int. Ed.* 59 (2020) 20582–20588.
- [5] K. Li, C.J. Liu, X.Z. Zhang, Multifunctional peptides for tumor therapy, *Adv. Drug Deliv. Rev.* 160 (2020) 36–51.
- [6] H.X. Liu, X.H. Chen, Y.M. Jia, H.Y. Chen, X.H. Wang, G.X. Liu, Y. Luo, Facing inevitable PARPis resistance: mechanisms and therapeutic strategies for breast cancer treatment, *Interdiscip. Med.* 1 (2023), e20220013.
- [7] H.Y. Bai, H.F. Wang, Z.H. Zhou, Y. Piao, X.R. Liu, J.B. Tang, X. Shen, Y.Q. Shen, Z. X. Zhou, Histone deacetylase-triggered self-immolative peptide-cytotoxins for cancer-selective drug delivery, *Adv. Funct. Mater.* (2023), 2214025.
- [8] X. Luan, H. Kong, P. He, G.Z. Yang, D.Z. Zhu, L. Guo, G. Wei, Self-assembled peptide-based nanodrugs: molecular design, synthesis, functionalization, and targeted tumor bioimaging and biotherapy, *Small* 19 (2023), 2205787.
- [9] Y.A. Sun, B. Lyu, C. Yang, B. He, H. Zhang, X.Q. Wang, Q. Zhang, W.B. Dai, An enzyme-responsive and transformable PD-L1 blocking peptide-photosensitizer conjugate enables efficient photothermal immunotherapy for breast cancer, *Bioact. Mater.* 22 (2023) 47–59.
- [10] Y.H. Ding, D.B. Zheng, L.M. Xie, X.Y. Zhang, Z.H. Zhang, L. Wang, Z.W. Hu, Z. M. Yang, Enzyme-instructed peptide assembly favored by preorganization for cancer cell membrane engineering, *J. Am. Chem. Soc.* 145 (2023) 4366–4371.
- [11] Y.M. Liu, R. Chang, R.R. Xing, X.H. Yan, Bioactive peptide nanodrugs based on supramolecular assembly for boosting immunogenic cell death-induced cancer immunotherapy, *Small Methods* (2023), 2201708.
- [12] S.R. Jia, S.L. Ji, J. Zhao, Y.H. Lv, J.Y. Wang, D.Q. Sun, D. Ding, A fluorinated supramolecular self-assembled peptide as nanovaccine adjuvant for enhanced cancer vaccine therapy, *Small Methods* (2023), 2201409.
- [13] Y.Y. Wu, H.N. Wen, Z.J. Bernstein, K.M. Hainline, T.S. Blakney, K.L. Congdon, D. J. Snyder, J.H. Sampson, L. Sanchez-Perez, J.H. Collier, Multipitope supramolecular peptide nanofibers eliciting coordinated humoral and cellular antitumor immune responses, *Sci. Adv.* 8 (2022) 7833.
- [14] M.Q. Sun, S.B. Yao, L.Y. Fan, Z.G. Fang, W.B. Miao, Z.Y. Hu, Z.H. Wang, Fibroblast activation protein- α responsive peptide assembling prodrug nanoparticles for remodeling the immunosuppressive microenvironment and boosting cancer immunotherapy, *Small* 18 (2022), 2106296.
- [15] M.D. Wang, D.Y. Hou, G.T. Lv, R.X. Li, X.J. Hu, Z.J. Wang, N.Y. Zhang, L. Yi, W. H. Xu, H. Wang, Targeted in situ self-assembly augmented peptide drug conjugate cell-entry efficiency, *Biomaterials* 278 (2021), 121139.
- [16] S. Soukasene, D.J. Toft, T.J. Moyer, H.M. Lu, H.K. Lee, S.M. Standley, V.L. Cryns, S. I. Stupp, Antitumor activity of peptide amphiphile nanofiber-encapsulated camptothecin, *ACS Nano* 5 (2011) 9113–9121.
- [17] Y.M. Zhang, Z.J. Feng, J.J. Liu, H. Li, Q. Su, J.M. Zhang, P.S. Huang, W.W. Wang, J. F. Liu, Polarization of tumor-associated macrophages by TLR7/8 conjugated radiosensitive peptide hydrogel for overcoming tumor radioresistance, *Bioact. Mater.* 16 (2022) 359–371.
- [18] T. Yu, W. Nie, Z.H. Hong, Y.H. He, J. Chen, X. Mi, S.P. Yang, X.L. Li, B.L. Wang, Y. Z. Lin, X. Gao, Synergy of immunostimulatory gene therapy with immune checkpoint blockade motivates immune response to eliminate cancer, *Adv. Funct. Mater.* 31 (2021), 2100715.
- [19] Y.H. Wang, J. Zhan, J.Y. Huang, X. Wang, Z.H. Chen, Z.M. Yang, Dynamic responsiveness of self-assembling peptide-based nano-drug systems, *Interdiscip. Med.* 1 (2023), 20220005.
- [20] W. Zhang, D.D. Li, X.D. Xu, Y. Chen, X.Y. Shi, Y.X. Pan, S.S. Yao, Y. Piao, Z.X. Zhou, N.K.H. Slater, Y.Q. Shen, J.B. Tang, A bispecific peptide-polymer conjugate bridging target-effector cells to enhance immunotherapy, *Adv. Healthcare Mater.* (2022), e2202977.
- [21] M.M. Li, Z.Y. Wang, X. Liu, N. Song, Y.Q. Song, X.F. Shi, J.J. Liu, J.F. Liu, Z.L. Yu, Adaptable peptide-based therapeutics modulating tumor microenvironment for combinatorial radio-immunotherapy, *J. Contr. Release* 340 (2021) 35–47.
- [22] M. Mamuti, Y. Wang, Y.D. Zhao, J.Q. Wang, J. Wang, Y.L. Fan, W.Y. Xiao, D. Y. Hou, J. Yang, R. Zheng, H.W. An, H. Wang, A polyvalent peptide CD40 nanoagonist for targeted modulation of dendritic cells and amplified cancer immunotherapy, *Adv. Mater.* 34 (2022), 2109432.
- [23] C.Y. Shi, Y. Wang, M.J. Wu, Y. Chen, F.Z. Liu, Z.Y. Shen, Y.R. Wang, S.F. Xie, Y. Y. Shen, L.J. Sang, Z. Zhang, Z.R. Gao, L.J. Yang, L. Qu, Z.Z. Yang, X.Y. He, Y. Guo, C.H. Pan, J.X. Che, H.Q. Ju, J. Liu, Z.J. Cai, Q.F. Yan, L.Y. Yu, L.J. Wang, X. W. Dong, P.L. Xu, J.Z. Shao, Y. Liu, X. Li, W.Q. Wang, R.H. Zhou, T.H. Zhou, A. F. Lin, Promoting anti-tumor immunity by targeting TMUB1 to modulate PD-L1 polyubiquitination and glycosylation, *Nat. Commun.* 13 (2022) 6951.

- [24] C.G. Buss, S.N. Bhatia, Nanoparticle delivery of immunostimulatory oligonucleotides enhances response to checkpoint inhibitor therapeutics, *Proc. Natl. Acad. Sci. U. S. A.* 117 (2020) 13428–13436.
- [25] Q.S. Hu, Y.Q. Ye, L.C. Chan, Y.J. Li, K. Liang, A.F. Lin, S.D. Egranov, Y.H. Zhang, W.Y. Xia, J. Gong, Y.H. Pan, S.S. Chatterjee, J. Yao, K.W. Evans, T.K. Nguyen, P. K. Park, J.W. Liu, C. Coarfa, S.R. Donepudi, V. Putluri, N. Putluri, A. Sreekumar, C. R. Ambati, D.H. Hawke, J.R. Marks, P.H. Gunaratne, A.S. Caudle, A.A. Sahin, G. N. Hortobagyi, F. Meric-Bernstam, L.P. Chen, D.H. Yu, M.C. Hung, M.A. Curran, L. Han, C.R. Lin, L.Q. Yang, Oncogenic lncRNA downregulates cancer cell antigen presentation and intrinsic tumor suppression, *Nat. Immunol.* 20 (2019) 835–851.
- [26] Z.L. Li, H. Cai, Z.Q. Li, L. Ren, X.L. Ma, H.Y. Zhu, Q.Y. Gong, H. Zhang, Z.W. Gu, K. Luo, A tumor cell membrane-coated self-amplified nanosystem as a nanovaccine to boost the therapeutic effect of anti-PD-L1 antibody, *Bioact. Mater.* 21 (2023) 299–312.
- [27] J. Li, Y. Fang, Y.F. Zhang, H.M. Wang, Z.M. Yang, D. Ding, Supramolecular self-assembly-facilitated aggregation of tumor-specific transmembrane receptors for signaling activation and converting immunologically cold to hot tumors, *Adv. Mater.* 33 (2021), 2008518.
- [28] F. Garrido, N. Aptsiauri, E.M. Doorduyn, A.M.G. Lora, T. van Hall, The urgent need to recover MHC class I in cancers for effective immunotherapy, *Curr. Opin. Immunol.* 39 (2016) 44–51.
- [29] Z. Liu, J.P. Li, Y. Jiang, D.D. Wang, Multifunctional nanocapsules on a seesaw balancing sonodynamic and photodynamic therapies against superficial malignant tumors by effective immune-enhancement, *Biomaterials* 218 (2019), 119251.
- [30] M.T. Liu, Z.Y. Cao, R.L. Zhang, Y.H. Chen, X.Z. Yang, Injectable supramolecular hydrogel for locoregional immune checkpoint blockade and enhanced cancer chemo-immunotherapy, *ACS Appl. Mater. Interfaces* 13 (2021) 33874–33884.
- [31] H.N. Li, J.Y. Sun, H.Y. Zhu, H.X. Wu, H. Zhang, Z.W. Gu, K. Luo, Recent advances in development of dendritic polymer-based nanomedicines for cancer diagnosis, *Wiley Interdiscip. Rev.: Nanomed. Nanobiotechnol.* 13 (2021), e1670.
- [32] X.Q. Wang, L. Ye, W.C. He, C.H. Teng, S.B. Sun, H.D. Lu, S.N. Li, L.Y. Lv, X. Cao, H. Y. Yin, W. Lv, H.L. Xin, In situ targeting nanoparticles-hydrogel hybrid system for combined chemo-immunotherapy of glioma, *J. Contr. Release* 345 (2022) 786–797.
- [33] W.Q. Jing, C. Chen, G.Y. Wang, M.S. Han, S.Z. Chen, X. Jiang, C.D. Shi, P. Sun, Z. M. Yang, B.K. Shi, X.Y. Jiang, Metabolic modulation of intracellular ammonia via intravesical instillation of nanoparticle-encased hydrogel eradicates bladder carcinoma, *Adv. Sci.* 10 (2023), e2206893.
- [34] J. Vansteenkiste, E. Wauters, Chemotherapy is strictly additive to immunotherapy, *J. Thorac. Oncol.* 14 (2019), S13–S13.
- [35] D. Tan, Chemotherapy directly targets the immune system to improve efficacy, *J. Thorac. Oncol.* 14 (2019), S14–S14.
- [36] Y.S. Cho, H. Kim, S.J. Park, S.W. Chung, Y.G. Ko, J.H. Yeo, J. Lee, S.K. Kim, J. U. Choi, S.Y. Kim, Y. Byun, Sustained potentiation of bystander killing via PTEN-loss driven macropinocytosis targeted peptide-drug conjugate therapy in metastatic triple-negative breast cancer, *Biomaterials* 289 (2022), 121783.
- [37] X.X. Han, K.M. Cheng, Y. Xu, Y.Z. Wang, H. Mm, Y.L. Zhang, X. Zhao, R.F. Zhao, G. J. Anderson, L. Ren, G.J. Nie, Y.Y. Li, Modularly designed peptide nanoprodug augments antitumor immunity of PD-L1 checkpoint blockade by targeting indoleamine 2,3-dioxygenase, *J. Am. Chem. Soc.* 142 (2020) 2490–2496.
- [38] Y.Y. Zhu, Y.Y. Huang, Y.L. Jin, S.L. Gui, R. Zhao, Peptide-guided system with programmable subcellular translocation for targeted therapy and bypassing multidrug resistance, *Anal. Chem.* 91 (2019) 1880–1886.
- [39] R. Chen, J.J. Wang, C. Qian, Y.J. Ji, C.Q. Zhu, L. Wu, W.D. Li, X.L. Bi, Y.T. Wang, G. Cao, Z.P. Chen, From nanofibers to nanorods: nanostructure of peptide-drug conjugates regulated by polypeptide-PEG derivative and enhanced antitumor effect, *Adv. Funct. Mater.* 29 (2019), 1806058.
- [40] Y.H. Hu, Y. Wang, J. Deng, X.Y. Ding, D.Q. Lin, H. Shi, L. Chen, D. Lin, Y.Q. Wang, S. Vakal, J.Q. Wang, X.Y. Li, Enzyme-instructed self-assembly of peptide-drug conjugates in tear fluids for ocular drug delivery, *J. Contr. Release* 344 (2022) 261–271.
- [41] Z.Y. Gong, B.L. Zhou, X.Y. Liu, J.J. Cao, Z.X. Hong, J.Y. Wang, X.R. Sun, X.M. Yuan, H.N. Tan, H.J. Ji, J.K. Bai, Enzyme-induced transformable peptide nanocarriers with enhanced drug permeability and retention to improve tumor nanotherapy efficacy, *ACS Appl. Mater. Interfaces* 13 (2021) 55913–55927.
- [42] Z.R. Wang, Y. Zhao, S. Zhang, X.H. Chen, G.M. Sun, B.L. Zhang, B. Jiang, Y.L. Yang, X.Y. Yan, K.L. Fan, Re-engineering the inner surface of ferritin nanocage enables dual drug payloads for synergistic tumor therapy, *Theranostics* 12 (2022) 1800–1815.
- [43] R.C. Guo, X.H. Zhang, P.S. Fan, B.L. Song, Z.X. Li, Z.Y. Duan, Z.Y. Qiao, H. Wang, In Vivo self-assembly induced cell membrane phase separation for improved peptide drug internalization, *Angew. Chem.-Int. Ed.* 60 (2021) 25128–25134.
- [44] X.L. Fan, J. Zhan, X.M. Pan, X. Liao, W.J. Guo, P.E. Chen, H.K. Li, W.J. Feng, Y. B. Cai, M.S. Chen, Enzymatic self-assembly nanofibers anchoring mesenchymal stem cells induce cell spheroids and amplify paracrine function for myocardial infarction therapy, *Chem. Eng. J.* 436 (2022), 135224.
- [45] L. Yang, R. Peltier, M. Zhang, D. Song, H. Huang, G. Chen, Y. Chen, F. Zhou, Q. Hao, L. Bian, M.L. He, Z. Wang, Y. Hu, H. Sun, Desuccinylation-triggered peptide self-assembly: live cell imaging of SIRT5 activity and mitochondrial activity modulation, *J. Am. Chem. Soc.* 142 (2020) 18150–18159.
- [46] H.L. Dong, M.S. Wang, S.H. Fan, C.A.L. Wu, C.H. Zhang, X. Wu, B. Xue, Y. Cao, J. J. Deng, D. Yuan, J.F. Shi, Redox-regulated conformational change of disulfide-rich assembling peptides, *Angew. Chem.-Int. Ed.* 61 (2022), e202212829.
- [47] M.D. Hade, C.N. Suire, Z.C. Suo, An effective peptide-based platform for efficient exosomal loading and cellular delivery of a microRNA, *ACS Appl. Mater. Interfaces* 15 (2023) 3851–3866.
- [48] C.H. Liang, X.R. Yan, R.S. Zhang, T.Y. Xu, D.B. Zheng, Z.Q. Tan, Y.X. Chen, Z. F. Gao, L. Wang, X.Y. Li, Z.M. Yang, Enhanced cellular uptake and nuclear accumulation of drug-peptide nanomedicines prepared by enzyme-instructed self-assembly, *J. Contr. Release* 317 (2020) 109–117.
- [49] C.E. Callmann, C.V. Barback, M.P. Thompson, D.J. Hall, R.F. Mattrey, N. C. Gianneschi, Therapeutic enzyme-responsive nanoparticles for targeted delivery and accumulation in tumors, *Adv. Mater.* 27 (2015) 4611–4615.
- [50] L. Gu, Z.Y. Duan, X. Li, X. Li, Y.G. Li, X.L. Li, G. Xu, P. Gao, H. Zhang, Z.W. Gu, J. Chen, Q.Y. Gong, K. Luo, Enzyme-triggered deep tumor penetration of a dual-drug nanomedicine enables an enhanced cancer combination therapy, *Bioact. Mater.* 26 (2023) 102–115.
- [51] D. Kalafatovic, M. Nobis, J.Y. Son, K.I. Anderson, R.V. Ulijn, MMP-9 triggered self-assembly of doxorubicin nanofiber depots halts tumor growth, *Biomaterials* 98 (2016) 192–202.
- [52] M.W. Cao, S. Lu, N.N. Wang, H. Xu, H. Cox, R.H. Li, T. Waigh, Y.C. Han, Y.L. Wang, J.R. Lu, Enzyme-triggered morphological transition of peptide nanostructures for tumor-targeted drug delivery and enhanced cancer therapy, *ACS Appl. Mater. Interfaces* 11 (2019) 16357–16366.
- [53] A. Tanaka, Y. Fukuoka, Y. Morimoto, T. Honjo, D. Koda, M. Goto, T. Maruyama, Cancer cell death induced by the intracellular self-assembly of an enzyme-responsive supramolecular gelator, *J. Am. Chem. Soc.* 137 (2015) 770–775.
- [54] J. Zhan, Y.B. Cai, S.S. He, L. Wang, Z.M. Yang, Tandem molecular self-assembly in liver cancer cells, *Angew. Chem. Int. Ed.* 57 (2018) 1813–1816.
- [55] Z.H. Peng, J. Kopecek, Enhancing accumulation and penetration of HPMA copolymer-doxorubicin conjugates in 2D and 3D prostate cancer cells via iRGD conjugation with an MMP-2 cleavable spacer, *J. Am. Chem. Soc.* 137 (2015) 6726–6729.
- [56] C.X. Fan, J.J. Shi, Y. Zhuang, L.L. Zhang, L. Huang, W. Yang, B. Chen, Y.Y. Chen, Z. F. Xiao, H. Shen, Y.N. Zhao, J.W. Dai, Myocardial-infarction-responsive smart hydrogels targeting matrix metalloproteinase for on-demand growth factor delivery, *Adv. Mater.* 31 (2019), 1902900.
- [57] B. Kim, G. Han, B.J. Toley, C.K. Kim, V.M. Rotello, N.S. Forbes, Tuning payload delivery in tumour cylindroids using gold nanoparticles, *Nat. Nanotechnol.* 5 (2010) 465–472.
- [58] J. Zhan, Y. Wang, S. Ma, Q. Qin, L. Wang, Y. Cai, Z. Yang, Organelle-inspired supramolecular nanomedicine to precisely abolish liver tumor growth and metastasis, *Bioact. Mater.* 9 (2022) 120–133.